Figures and figure supplements

Molecular tuning of sea anemone stinging

Lily S He *et al*.

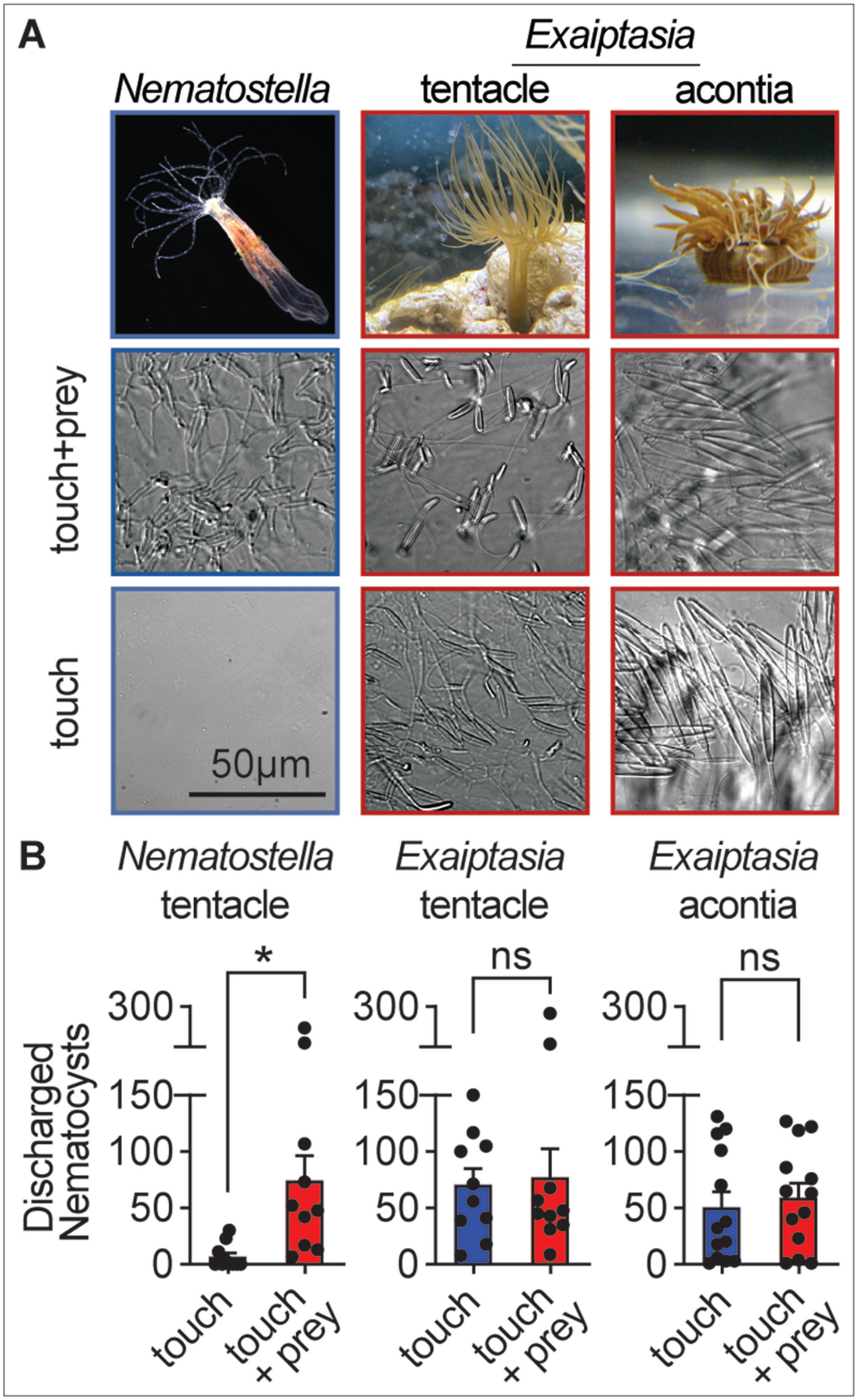

Figure 1. Comparative sea anemone stinging behavior. (**A**) *Nematostella vectensis* stings with tentacles while *Exaiptasia diaphana* also stings with acontia filaments that are ejected from its body for defense. *Left: Nematostella* nematocyte discharge was only observed in response to simultaneous prey chemicals and touch stimuli. *Middle, Right: Exaiptasia* nematocyte discharge from tentacles and acontia occurred irrespective of prey

Figure 1 continued on next page

Figure 1 continued

cues (touch alone). Scale bar = 50 μm. (**B**) *Nematostella* nematocyte discharge was elicited by simultaneous touch and prey chemical stimuli (n=10 trials). *Exaiptasia* tentacle (n=10) and acontia (n=13) nematocytes discharged only to touch, with or without prey chemicals. $p<0.05$ for *Nematostella*, paired two-tailed student's t-test. Data represented as mean ± sem.

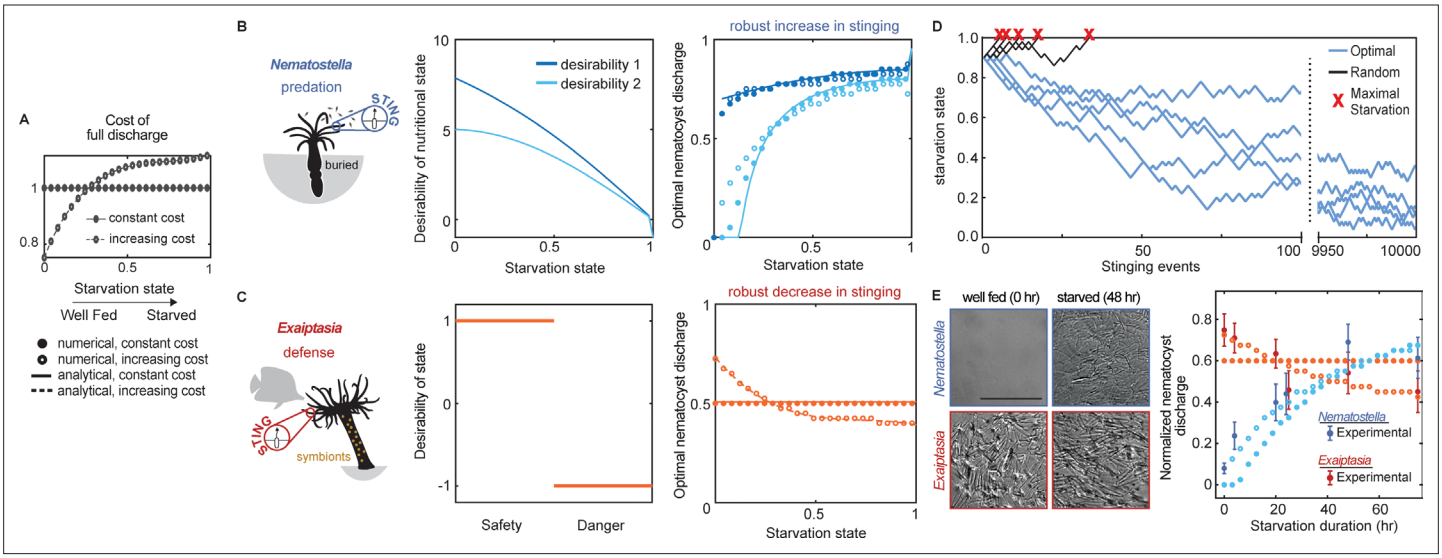

Figure 2. *Nematostella* stinging is regulated by predation while *Exaiptasia* stings for defense. (**A**) The cost of stinging is $c = c_o a$, where c_o is the cost for full nematocyte discharge and it either does not change (solid lines filled circles) or increases slightly (dashed lines empty circles) with starvation state. These symbols are used throughout the figure to represent each cost function. The increasing cost is obtained by fitting the Exaiptasia behavior (*see fitting procedure in Materials and methods*). (**B**) *Left: Nematostella* burrows in the substrate and stings for predation. *Center*: Desirability of nutritional state, or reward, decreases with starvation. Two examples are shown: example 1, $r\left(s\right) = 10tan^{-1}\left(1-s\right)$; example 2, $r\left(s\right) = 5cos\left(\frac{s\pi}{2}\right)$. *Right*: Predicted optimal stinging obtained by solving ***equation (1)*** with numerical simulations (circles) and approximate analytical solutions (lines) assuming: $p\left(a\right) = p_M a\left(2-a\right)$ and $p_M = 0.8$; $c = c_0 a$ with cost for full discharge c_0 matching panel A (full circles and solid lines for constant cost; empty circles for increasing cost); reward in Left panels (colors match). For all reward and cost functions, optimal predatory stinging increases with starvation under broad assumptions (*see Materials and methods*). (**C**) *Left: Exaiptasia diaphana* relies heavily on endosymbiotic algae for nutrients and stings primarily for defense. *Center:* We assumed there are two states, safety (L), and danger (**D**). The state of safety can transition to danger, but not the other way around. We assumed the agent obtains reward 1 in state L and penalty –1 in state D. *Right:* Predicted optimal stinging obtained by solving ***equation (2)*** with numerical simulations (circles) and analytical solutions (lines). Styles match the costs in panel A; we assume $p\left(a\right) = p_M a\left(2-a\right)$ and $p_M = 0.8$ as before. Optimal defensive stinging is constant or decreases with starvation under broad assumptions (*see Materials and methods*). (**D**) Examples of optimal (blue) versus random (black) predatory stinging. Each agent (anemone) starts with $s = 0.9$, and stings sequentially for many events (represented on the *x* axis). The random agent almost always reaches maximal starvation before 50 events (grey lines, five examples shown). In comparison, the optimal agent effectively never starves due to a successful stinging strategy optimized for predation (blue lines, five examples shown, parameters as in panel B, curve with matching color). (**E**) *Left: Nematostella* nematocyte discharge was affected by prey availability while *Exaiptasia* stung at a similar rate regardless of feeding. p<0.0001 for *Nematostella*, two-way ANOVA with post hoc Bonferroni test (n=10 animals, data represented as mean ± sem). *Right*: Experimental data (circles with error bars representing standard deviation) are well fit by normalized optimal nematocyst discharge predicted from MDP models for both *Exaiptasia* (orange full and empty circles for constant and increasing cost, panel A) and *Nematostella* (light blue full and empty circles for constant and increasing cost, panel A and desirability 2 in panel B). We match the last experimental data point to $s = 0.5$, the precise value of this parameter is irrelevant as long as it is smaller than 1, representing that animals are not severely starved during the experiment.

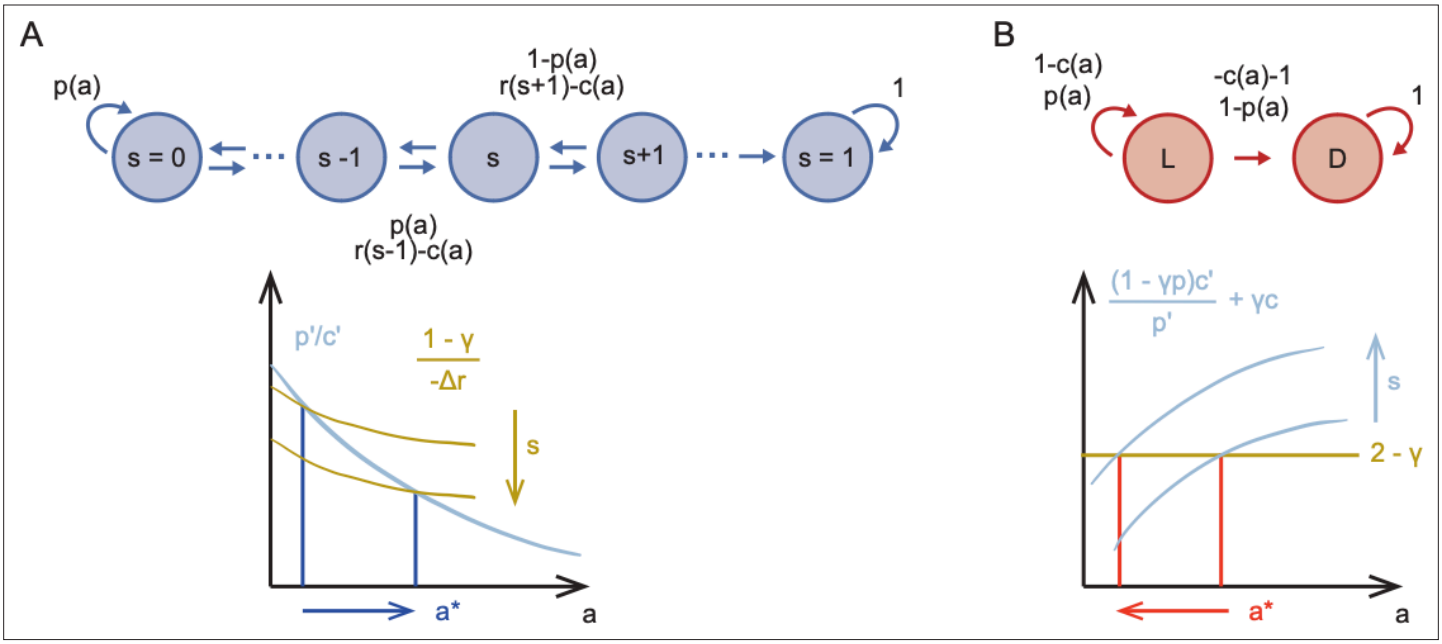

Figure 2—figure supplement 1. Sketch of Markov Decision Processes model and predictions for stinging. (**A**) Directed graph representing the Markov Decision Process for predatory stinging (*top*) including states of starvation s, actions a, and transitions to adjacent states depending on the probability to catch prey $p\left(a\right)$. Graphical representation of the result that optimal predatory stinging increases with starvation (*bottom*). (**B**) Directed graph representing the Markov Decision Process for defensive stinging (*top*) including states of safety and danger L and D, actions a, and transitions between L and D depending on the probability to successfully stinging the predator $p\left(a\right)$. Graphical representation of the result that the optimal defensive stinging decreases with starvation (*bottom*).

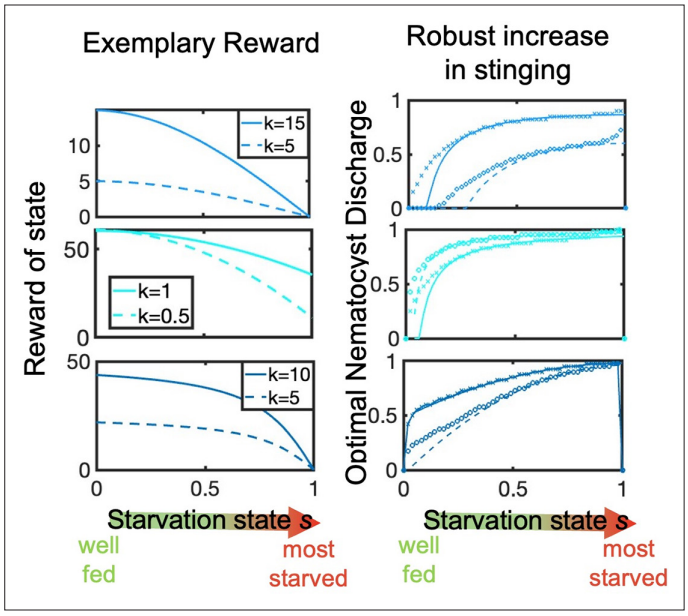

Figure 2—figure supplement 2. Optimal policy predicted by Bellman's theory for the MDP sketched in ***Figure 2—figure supplement 1A***. *Left*: three choices of concave reward functions $r\left(s'\right):r\left(s\right)=kcos\left(s\pi/2\right)$, upper left; $r=k\left(1-50s2\right)+60$, middle left; $r=ktan-1$, lower left. Solid and dashed lines correspond to two choices of the parameter k for each reward as in the legend. The cost of full dischare is constant $c_0=1.5$ and the likelihood of successful discharge is $p=p_Ma\left(2-a\right)$ with $p_M=0.6$. *Right*: the asymptotic solution for the optimal policy $a\left(s\right)$ (solid and dashed lines matching the corresponding reward on the left) reproduces well the numerical solution obtained from solving Bellman's ***Equation (1)*** with the value iteration algorithm (crosses and circles correspond to the solid and dashed rewards on the left). Optimal nematocyst discharge increases with the starvation state, independently on the shape of the reward function.

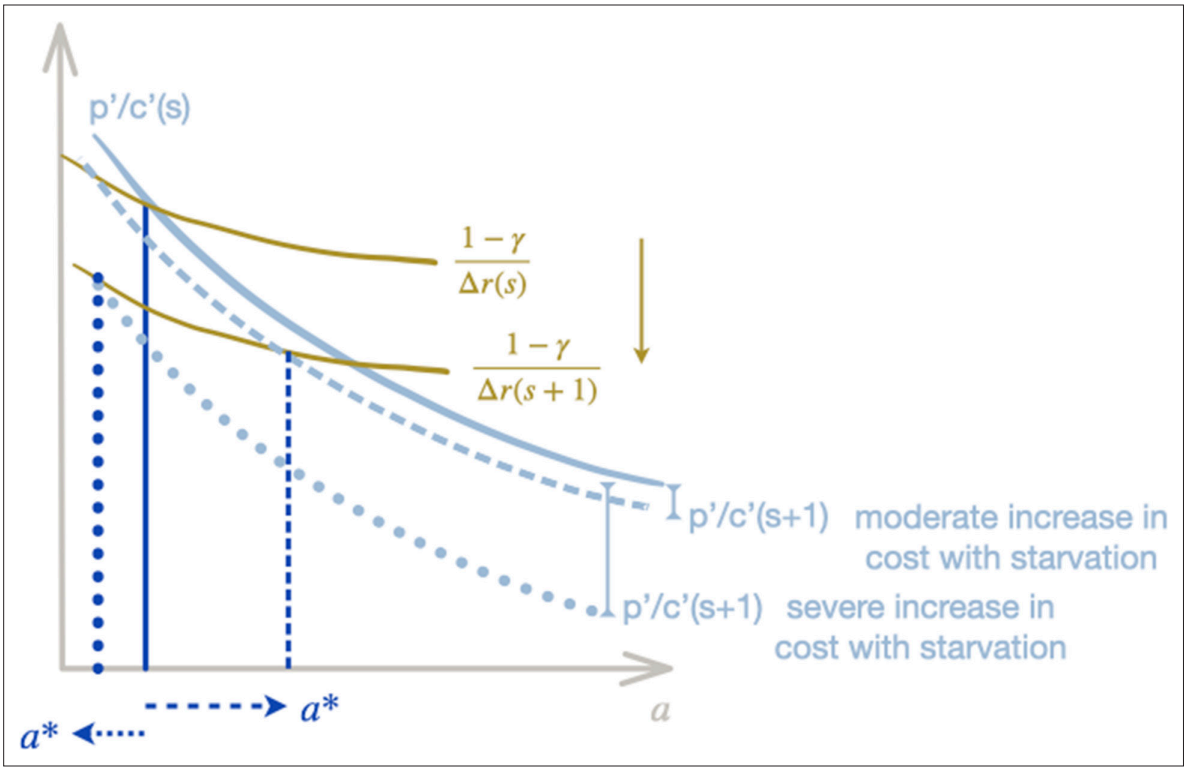

Figure 2—figure supplement 3. Sketch of theoretical prediction for predatory stinging with increasing cost. Similar to ***Figure 2—figure supplement 1A*** bottom, for the case where the cost per nematocyte varies with starvation $c = c_0\ (s)\ a$. Moderate increase in the cost per starvation (dashed light-blue line) do not affect the qualitative results as the green curve still intersects the light-blue curve for increasing values of a(marked by dashed dark-blue line). More dramatic increases of cost with starvation (light-blue dotted line) do lead to a decrease in predatory stinging with starvation as the intercept now moves backward with increasing s(marked by dark-blue dotted line).

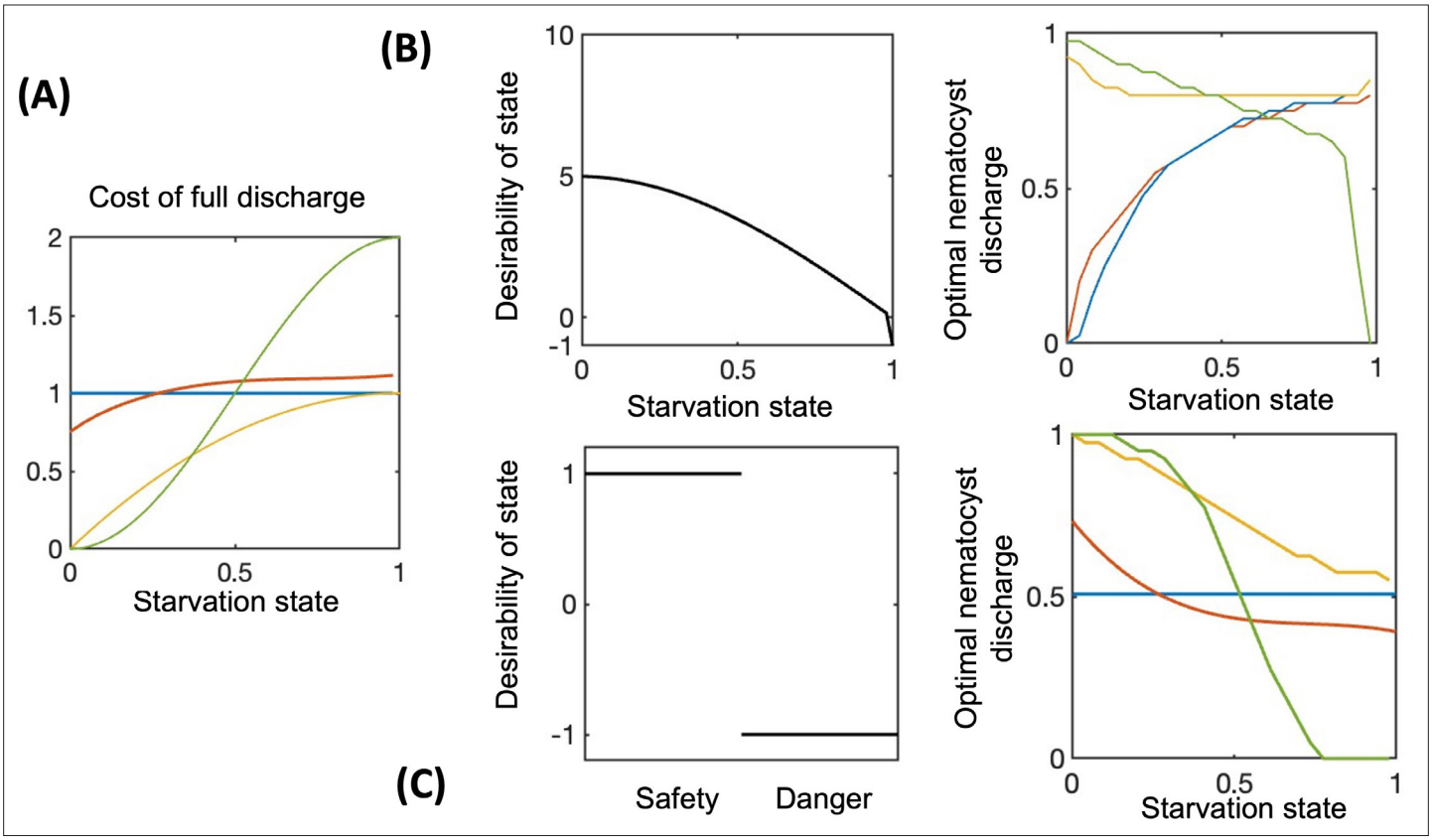

Figure 2—figure supplement 4. Effects of a moderately *vs* dramatically increasing cost with starvation. For a constant cost of full discharge or moderately increasing cost with starvation, predatory stinging always increases, whereas defensive stinging decreases or stays constant (results discussed in main text, ***Figure 2***, and reproduced here for comparison, red and blue curves in Panels **A-C**. For predation, we use desirability 2 from ***Figure 2B***). When the cost function increases dramatically with starvation (panel **A**, yellow and green lines), defensive stinging keeps decreasing with starvation (panel **C**, right), but now also predatory stinging decreases with starvation (panel **B**, right, yellow and green lines). Results are obtained with numerical simulations.

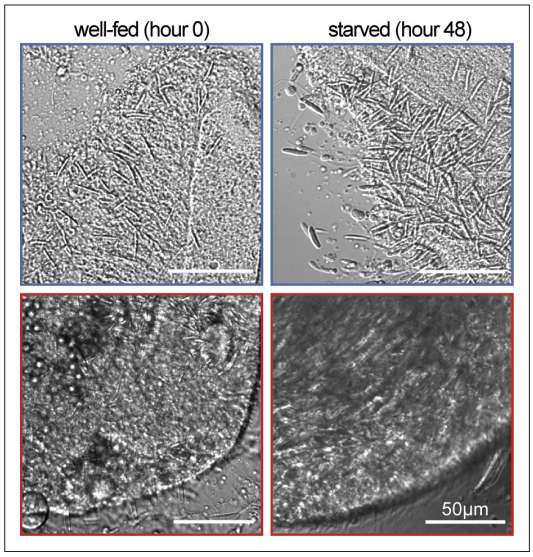

Figure 2—figure supplement 5. Modulation of *Nematostella* and *Exaiptasia* stinging is not due to changes in the abundance of nematocytes. Nematocytes were highly abundant in tentacles from *Nematostella (top)* and *Exaiptasia (bottom)* before and after starvation. Representative of n=3 animals. Scale bar = 50 µm.

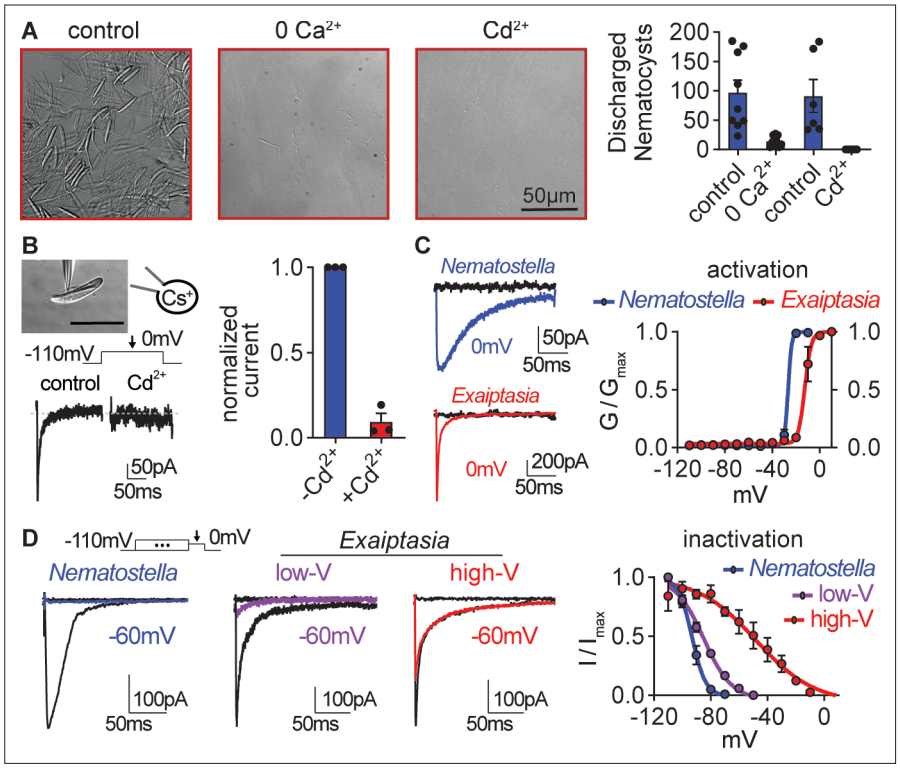

Figure 3. *Exaiptasia* nematocyte voltage-gated Ca^{2+} currents exhibit minimal steady-state inactivation compared with *Nematostella*. (**A**) Touch-elicited *Exaiptasia* tentacle nematocyte discharge was blocked in the absence of Ca^{2+} ($p<0.01$, paired two-tailed student's t-test, n=9 animals) or by addition of the Ca_V channel blocker Cd^{2+} (500 µM, $p<0.05$, paired two-tailed student's t-test, n=6 animals). Scale bar = 50 µm. (**B**) *Top:* Representative patch clamp experiment from an *Exaiptasia* nematocyte. Scale bar = 20 µm. *Bottom:* Nematocyte voltage-gated currents elicited by a maximally activating 0 mV pulse were blocked by Cd^{2+} (n=3 cells, $p<0.01$, paired two-tailed student's t-test). (**C**) Nematocyte voltage-gated currents elicited by –120 mV (black) or 0 mV pulses (colored). Conductance-voltage curves for *Nematostella* nematocyte ($V_{a1/2}$ = -26.54 ± 0.78mV, n=3) and *Exaiptasia* nematocyte ($V_{a1/2}$ = -12.47 ± 0.70mV, n=3). (**D**) Nematocyte voltage-gated currents elicited by a maximally activating voltage pulse following 1 s pre-pulses to −110 mV (max current, black), −50 mV (colored), or 20 mV (inactivated, no current). *Nematostella* nematocytes inactivated at very negative voltages ($V_{i1/2}$ = -93.22 ± 0.42mV, n=7) while *Exaiptasia* contained two populations of nematocytes: low-voltage threshold ($V_{i1/2}$ = -84.94 ± 0.70mV, n=4), and high-voltage threshold ($V_{i1/2}$ = -48.17 ± 3.32mV, n=3). Data represented as mean ± sem.

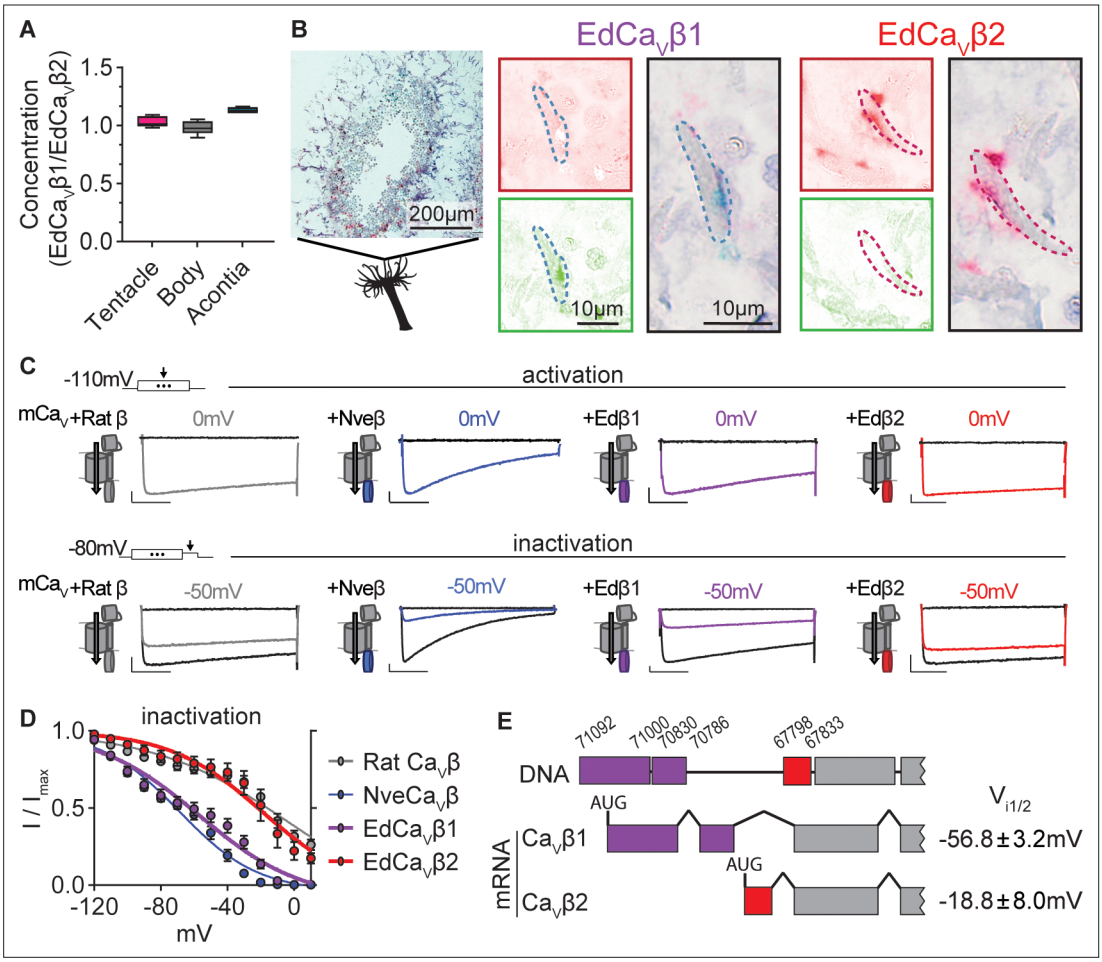

Figure 4. *Exaiptasia* expresses a Ca_V β subunit splice isoform that confers weak voltage-dependent inactivation. (**A**) ddPCR ratio of concentrations of Ca_V β subunit 1 and 2 mRNAs was similar in tentacle (n=5), body (n=5), and acontia (n=4 animals) tissue samples. (**B**) $EdCa_V\beta1$ and $EdCa_V\beta2$ localized to distinct nematocytes in *Exaiptasia* tentacle cross section, as visualized by BaseScope in situ hybridization. Representative nematocyte expressing $EdCa_V\beta1$ (green) or $EdCa_V\beta2$ (red). Representative of three animals. (**C**) Voltage-gated currents from heterologously-expressed chimeric mammalian Ca_V (mCa_V) with different β subunits: rat (*Rattus norvegicus*), *Nematostella* (Nve), *Exaiptasia* $EdCa_V\beta1$ or $EdCa_V\beta2$. *Top*: Currents elicited by voltage pulses to –120 mV (no current, black) and maximally activating 0 mV (colored). *Bottom*: Voltage-gated currents elicited by a maximally activating voltage pulse following 1 s pre-pulses to −110 mV (max current, black), −50 mV (colored), or 20 mV (inactivated, no current, black). Scale bars = 100 pA, 50ms. (**D**) *Exaiptasia* Ca_V β subunit splice isoforms confer distinct inactivation: *Nematostella* β subunit ($V_{i1/2}$ = -68.93 ± 1.53mV, n=5) and Rat β2a subunit ($V_{i1/2}$ = -2.98 ± 13.51mV, n=12) and $EdCa_V\beta1$ ($V_{i1/2}$ = -56.76 ± 3.18mV, n=8), and $EdCa_V\beta2$ ($V_{i1/2}$ = -18.84 ± 8.00mV, n=5 cells). Data represented as mean ± sem. (**E**) Genomic alignment of *Exaiptasia* β subunit isoforms showed that alternative splicing of the N-terminus region was associated with distinct inactivation: $Ca_V\beta1$ (long N-term) had low-voltage steady-state inactivation similar to *Nematostella*, while $Ca_V\beta2$ (short N-term) exhibited more depolarized steady-state inactivation, matching its mammalian orthologue. Genomic loci listed above sequence.

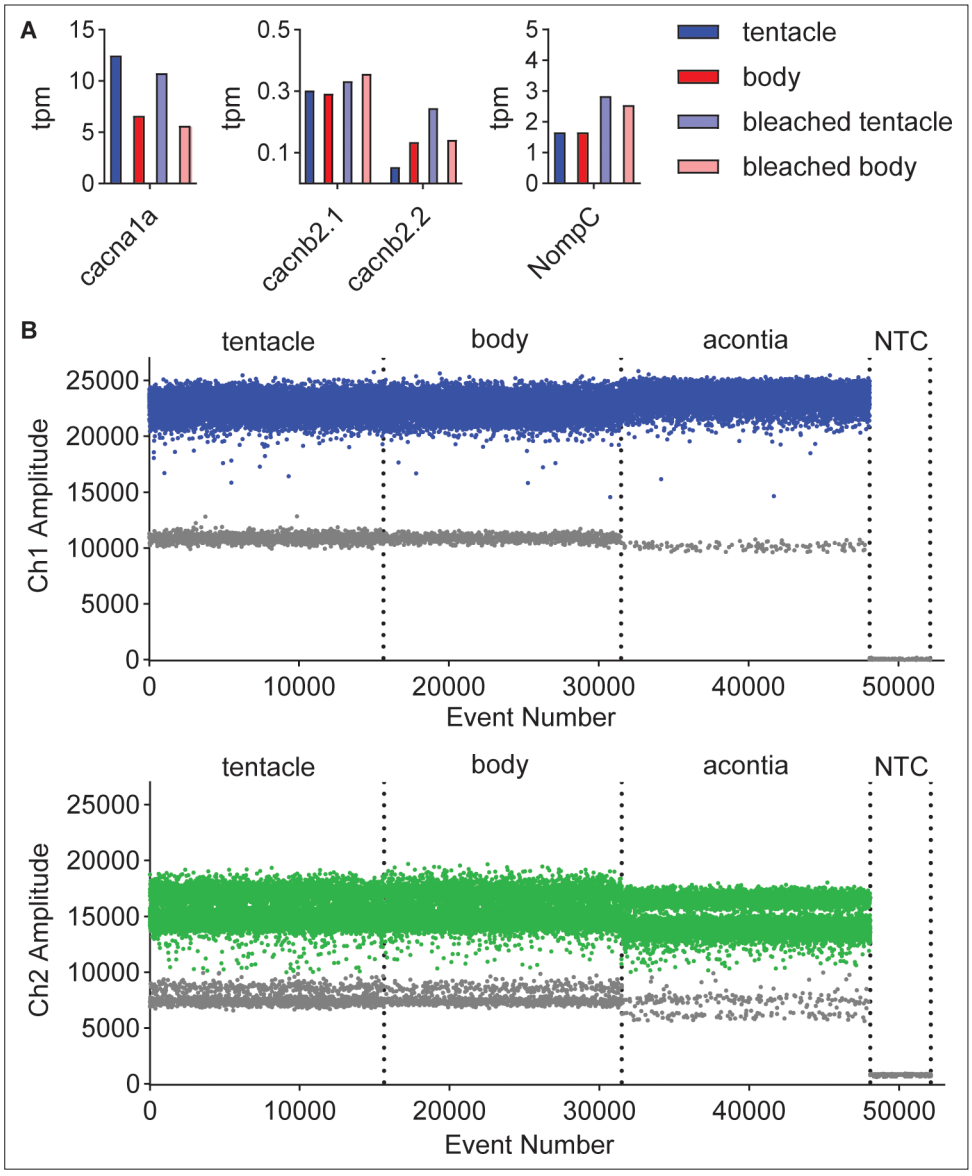

Figure 4—figure supplement 1. Transcriptomic and molecular analyses of *Exaiptasia* β subunit isoforms. (**A**) mRNA expression (transcripts per million, TPM) of voltage-gated calcium (Ca_V) channel α and β subunits in *Exaiptasia* tentacle (nematocyte abundant, blue), body (nematocyte non-abundant, red), bleached (minimal symbionts) tentacle (light blue), bleached body (light red) tissues. The Ca_V α subunit was identified by homology to the sequence of the cnidarian $Ca_V2.1$ homolog found enriched in *Nematostella* nematocyte-rich tissues (***Weir et al., 2020***). NompC, the putative mechanoreceptor in *Nematostella* nematocytes (***Schüler et al., 2015***; ***Weir et al., 2020***), was also detected in *Exaiptasia* tentacles. (**B**) Representative plots of fluorescent amplitude across event number (droplet events) from amplification of unique regions of EdCa_Vβ1 (Ch1, *Top*) and EdCa_Vβ2 (Ch2, *Bottom*) sequences using droplet digital PCR (ddPCR, Bio-Rad Laboratories). Individual lanes correspond to tentacle RNA, body RNA, acontia RNA, and no template control (NTC). Blue and green points indicate positive PCR droplets after thresholding and gray points indicate negative droplets.

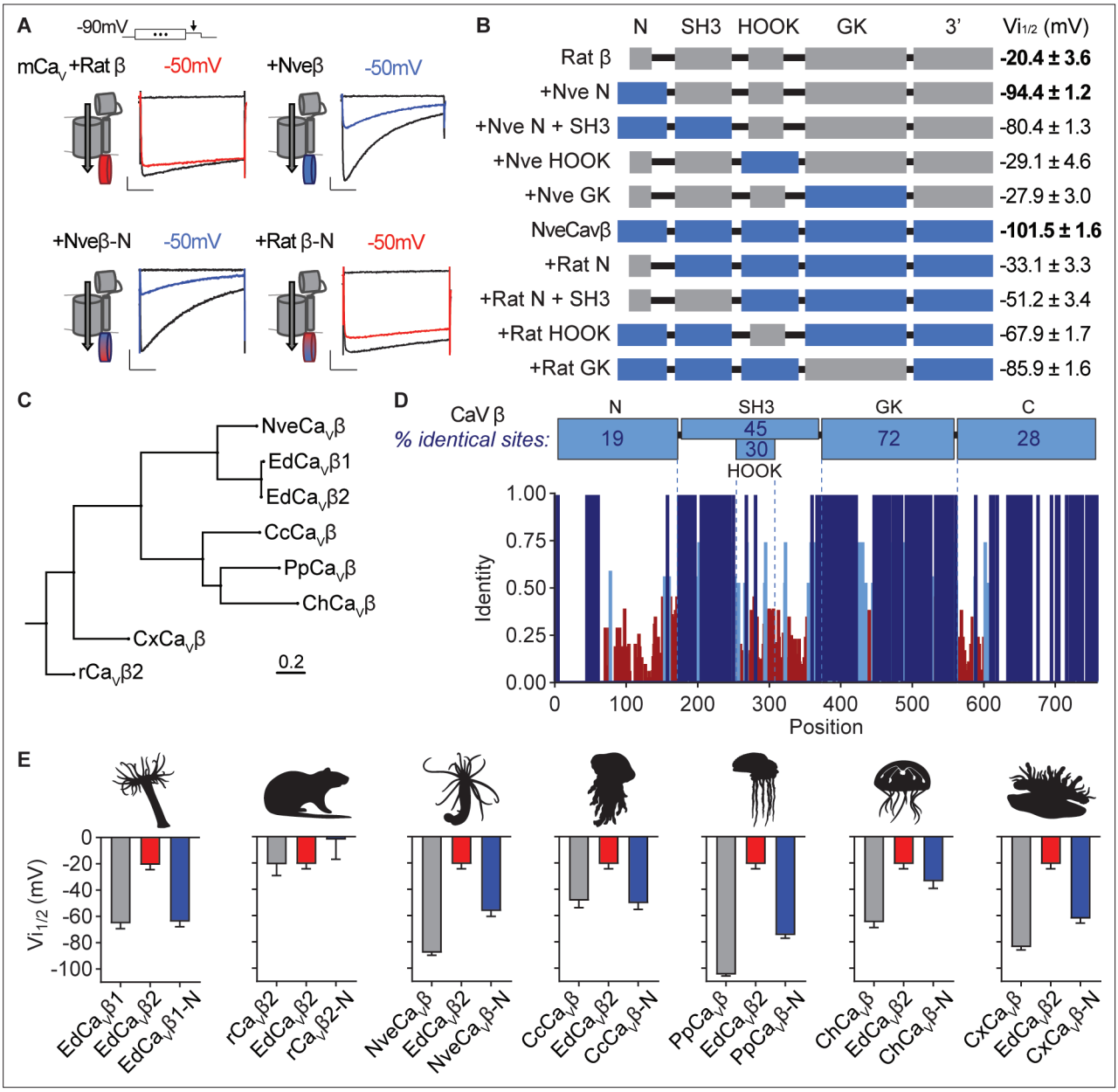

Figure 5. Cnidarian Ca_V β subunit N-termini confer unique inactivation properties. (**A**) Voltage-gated currents from heterologously expressed Ca_V channels with *Nematostella*-rat chimeric β subunits demonstrate that the *Nematostella* N-terminus is sufficient to drive inactivation at negative voltages. Currents shown in response to 10 mV voltage pulses following 1 s pre-pulses to −130 mV (max current, black), −50 mV (colored), or 0 mV (inactivated, no current, black). Scale bars = 100 pA, 50ms. (**B**) Diagram of Ca_V *Nematostella*-rat β subunit domain swaps and resulting $V_{i1/2}$ values. The *Nematostella* β subunit N-terminus is required and sufficient for uniquely hyperpolarized Ca_V inactivation properties ($p<0.001$ for average $V_{i1/2}$ values across mutant beta subunits, one-way ANOVA with post-hoc Tukey test, n=2–8 cells). (**C**) Phylogenetic tree of β subunit sequences obtained from several species of cnidarians. Abbreviations of species: Nve, *Nematostella vectensis*; Ed, *Exaiptasia diaphana*; Cc, *Cyanea capillata* (jellyfish); Pp, *Physalia physalis* (siphonophore); Ch, *Clytia hemisphaerica* (jellyfish); Cx, *Cassiopea xamachana* (jellyfish); r, *Rattus norvegicus*. (**D**) *Top*: Percentage of identity between amino acid sequences across β subunit protein domains for $NveCa_V\beta$, $EdCa_V\beta1$, $EdCa_V\beta2$, $CcCa_V\beta$, $PpCa_V\beta$, $ChCa_V\beta$, $CxCa_V\beta2$, $rCa_V\beta2$. *Bottom*: Fraction of identity of amino acids across sites of the β subunit protein. (**E**) Cnidarian Ca_V β N-termini shift depolarized, weak voltage-dependent inactivation of Ca_V channels containing $EdCa_V\beta2$ to more negative voltages. Voltage-dependent inactivation ($V_{i1/2}$) of heterologously-expressed Ca_Vs with WT $EdCa_V\beta2$, β subunits from the indicated cnidarians, and chimeras with their N-termini on $EdCa_V\beta2$ ($p<0.0001$ for average $V_{i1/2}$ values with multiple comparisons against WT $EdCa_V\beta2$ mean, one-way ANOVA with Bartlett's test and post-hoc Tukey test, n=4–9 cells). Data represented as mean ± sem.

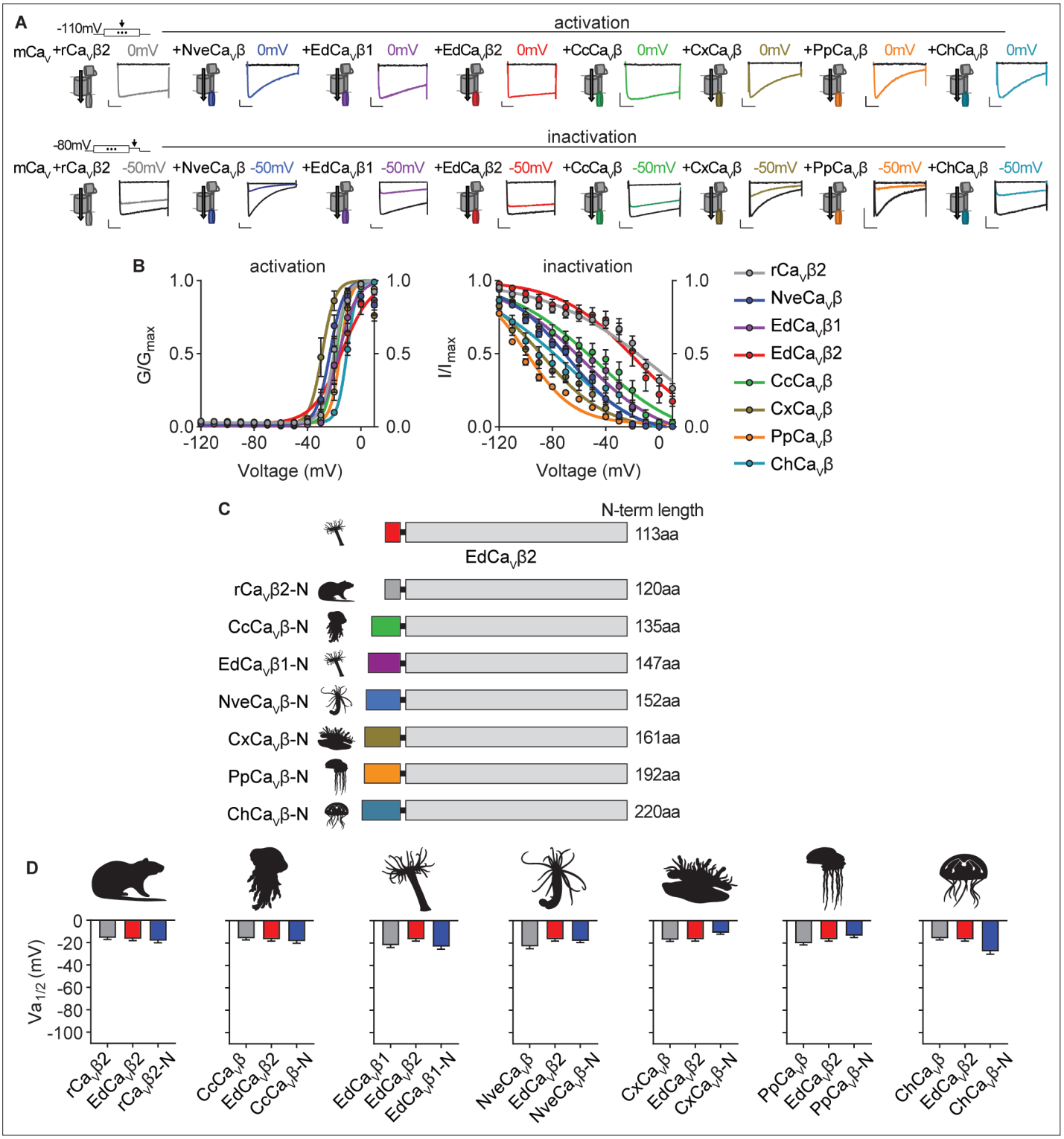

Figure 5—figure supplement 1. Voltage-dependent activation of Ca_V channels is conserved across cnidarian β subunits. (**A**) *Top*: Voltage-gated currents from heterologously-expressed chimeric Ca_Vs with the indicated β subunits elicited by voltage pulses to –120 mV (no current, black) and 0 mV (colored). Abbreviations of species: Nve, *Nematostella vectensis*; Ed, *Exaiptasia diaphana*; Cc, *Cyanea capillata* (jellyfish); Pp, *Physalia physalis* (siphonophore); Ch, *Clytia hemisphaerica* (jellyfish); Cx, *Cassiopea xamachana* (jellyfish); r, *Rattus norvegicus*. *Bottom*: Voltage-gated currents elicited by a maximally activating voltage pulse following 1 s pre-pulses to −110 mV (max current, black), −50 mV (colored), or 20 mV (inactivated, no current, black). Scalebars = 100 pA, 50ms. (**B**) Activation and inactivation curves for heterologously-expressed chimeric Ca_Vs with different β subunits. Activation: rCaVβ2 $V_{a1/2}$ = -19.76 ± 1.16mV, n=12; NveCaVβ $V_{a1/2}$ = -23.07 ± 1.16mV, n=5; EdCaVβ1 $V_{a1/2}$ = -18.27 ± 1.08mV, n=8; EdCaVβ2 $V_{a1/2}$ = -14.22 ± 1.46mV, n=5;

Figure 5—figure supplement 1 continued on next page

Figure 5—figure supplement 1 continued

$CcCa_V\beta$ $V_{a1/2}$ = -18.47 ± 1.59mV, n=6; $CxCa_V\beta$ $V_{a1/2}$ = -28.89 ± 1.54mV, n=15; $PpCa_V\beta$ $V_{a1/2}$ = -15.29 ± 1.23mV, n=10; $ChCa_V\beta$ $V_{a1/2}$ = -10.30 ± 1.04mV, n=12. $rCa_V\beta2$ $V_{i1/2}$ = -2.98 ± 13.51mV, n=12; $NveCa_V\beta$ $V_{i1/2}$ = -68.93 ± 1.53mV, n=5; $EdCa_V\beta1$ $V_{i1/2}$ = -56.76 ± 3.18mV, n=8; $EdCa_V\beta2$ $V_{i1/2}$ = -18.84 ± 8.00mV, n=5; $CcCa_V\beta$ subunit $V_{i1/2}$ = -47.81 ± 5.57mV, n=6; $CxCa_V\beta$ $V_{i1/2}$ = -87.75 ± 1.72mV, n=15; $PpCa_V\beta$ $V_{i1/2}$ = -99.80 ± 0.92mV, n=10; $ChCa_V\beta$ $V_{i1/2}$ = -70.25 ± 4.67mV, n=12 cells. (**C**) Diagram of Ca_V β subunit domain swaps and the length of the N-terminus swapped in amino acids. (**D**) Cnidarian Ca_V β N-termini do not greatly affect voltage-dependent activation of Ca_V channels containing $EdCa_V\beta2$. Voltage-dependent activation ($V_{a1/2}$) of heterologously-expressed Ca_Vs with WT $EdCa_V\beta2$, β subunits from the indicated cnidarians, and chimeras with their N-termini on $EdCa_V\beta2$, p=0.5830 for average $V_{i1/2}$ values across mutant beta subunits, one-way ANOVA with Bartlett's test and post-hoc Tukey test, n=4–7 cells. Data represented as mean ± sem.